Thermoconvective instabilities of 2D Poiseuille-Rayleigh-Bénard for supercritical fluids in micro/macro-channels

D. Ameur, I. Raspo, J. Dib

THERMOCONVECTIVE INSTABILITIES OF 2D POISEUILLE-RAYLEIGH-BENARD FOR SUPERCRITICAL FLUIDS IN MICRO/MACRO-CHANNELS

D. Ameur[1*], I. Raspo[2], J. Dib[1]

[1]University of Abou Bekr Belkaid Tlemcen, Materials and Renewable Energy Research Unit, Faculty of sciences, Algeria

[2]Aix-Marseille University, CNRS, Centrale Marseille, M2P2 UMR 7340 Technopôle de Château-Gombert, 13451 Marseille Cedex 20, France

[1*]e-mail address: d.ameur@yahoo.fr

[2]e-mail address: isabel@l3m.univ-mrs.fr

[1]e-mail address: joannadib2022@yahoo.fr

Corresponding author: D. Ameur

ABSTRACT

The objective of this paper is to study the influence of specific properties of supercritical fluid on the thermoconvective instabilities phenomena comparatively with those observed in the ideal gases case. This study concerns the mixed convection in a supercritical fluid flowing in a millimetric channel heated from below and traversed by a supercritical flow CO_2. The dependence of the instability threshold on the Reynolds and Prandtl numbers is investigated as well as the characteristics of the thermoconvective structures for a large range of the relevant dimensionless parameters. The study is carried out by direct numerical simulations based on the solution of the Navier-Stokes equations, coupled with the energy equation and the Peng-Robinson equation of state, in the framework of the low Mach number

approximation. Simulations were performed for Reynolds numbers ranging from 12 up to 101. The instability threshold was determined from numerical solutions for several values of *Re* and it was found to vary as a fourth degree polynomial of *Re.*

KEY WORDS: Mixed convection flows, Poiseuille-Rayleigh-Bénard flows, thermoconvective instability, supercritical fluid, numerical simulation, spectral methods.

NOMENCLATURE

a	[-]	Energy parameter in the equation of state
b	[-]	Covolume in the equation of state
C_P'	[J/(kg.K)]	Isobaric specific heat
C_V'	[J/(kg.K)]	Isochoric specific heat
g'	[m/s^2]	Gravity constant
H'	[m]	Channel height
L'	[m]	Channel length
P'	[Pa]	pressure
R'	[J/(kg.K)]	Perfect gas constant
t'	[s]	Time
T'	[K]	Temperature
u'	[m/s]	Velocity component in the x-direction
v'	[m/s]	Velocity component in the y-direction
x'	[m]	Cartesian axis direction
y'	[m]	Cartesian axis direction

Special characters

α	[-]	Soave function in the equation of state
β'	[K^{-1}]	Thermal expansion coefficient
δt	[-]	Dimensionless time step
$\delta T'$	[K]	Temperature increase
ε	[-]	Dimensionless proximity to the critical point, $\varepsilon = \left(T_i' - T_c'\right)/T_c'$
λ'	[W/(m.K)]	Thermal conductivity
μ'	[Pa.s]	Dynamic viscosity
ρ’	[kg/m^3]	Density
χ'	[Pa^{-1}]	Isothermal compressibility
ω	[-]	Acentric factor
Ω	[-]	Computational domain
$\partial\Omega$	[-]	Boundary of the computational domain
γ	[-]	Specific heats ratio

Subscripts

b	Background property
c	Critical property
dyn	Dynamic part
hyd	Hydrostatic part
i	Initial value
mean	Mean value

ref	Reference value
th	Thermodynamic part
0	Value for the perfect gas

1. INTRODUCTION AND FORMULATION PROBLEM

The study of the famous Poiseuille-Rayleigh-Bénard (PRB) problem for ideal fluids, involving the onset of thermoconvective structures in ducts uniformly heated from below, was the subject of several studies. However, the corresponding problem of thermal instability in PRB configuration for supercritical fluid (SF) has never been studied to our knowledge. Near the liquid-gas critical point, the fluid thermophysical properties are intermediate between those of gases and liquids (for instance, viscosity and diffusivity are similar to those of gases while density is alike that of liquids). Moreover, they are continually adjustable with small variations of temperature and pressure. This flexibility motivated the use of supercritical fluids (namely fluids with temperature and pressure exceeding the critical coordinates) in many industrial applications, (Reverchon and De Marco, 2006; Cocero et al., 2009; Cansell and Aymonier, 2009). The stability of PRB flows depends on three dimensionless parameters: the Rayleigh Ra, the Reynolds Re and the Prandtl Pr numbers. When the Rayleigh number exceeds a critical value for fixed Reynolds and Prandtl numbers, thermoconvective structures develop in the channel. The instability onset and the development of the associated patterns in PRB flows were extensively studied for incompressible fluids and perfect gas from many years because of the practical but also fundamental interests of this problem. Nicolas (2002) showed that, when the base flow becomes unstable, mainly two kinds of thermoconvective structures may appear: transversal rolls at low Reynolds number (about $Re<10$) and longitudinal rolls at higher Reynolds number. Transversal rolls are travelling rolls with axis perpendicular to the mean flow direction and these patterns can be considered as a quasi two-

dimensional structure, whereas longitudinal rolls consist of helicoidal rolls aligned with the flow direction and the three velocity components are excited. More complex thermoconvective structures, such as superposition of transversal and longitudinal rolls or wavy longitudinal rolls (Nicolas et al., 2012), among others, were also observed.

Results of linear stability analysis for incompressible flows showed that the transversal rolls are due to a convective or an absolute instability depending on the value of the Rayleigh number (Müller et al., 1992; Carrière and Monkewitz, 1999). When the flow is linearly convectively unstable, the downstream and upstream fronts of the perturbation spread in the mean flow direction. In the relative reference frame moving with the perturbation, the perturbation amplitude grows with time but, for sufficiently long times, it locally decreases at each axial position. The perturbation finally leaves the system and the flow becomes stable again. On the other hand, in the case of an absolute instability, the initial perturbation locally grows but it also expands in the whole system so that the rolls appear throughout the channel all the time although they move downstream: when a roll moves away, another one is locally generated in its place by the perturbation. For fixed Reynolds *Re* and Prandtl *Pr* numbers, the convective or absolute nature of the instability depends on the value of the Rayleigh number *Ra*. The critical Rayleigh numbers for the onset of convective instability, Ra_{c1}, and of absolute instability, Ra_{c2}, were theoretically established as a function of the Reynolds and Prandtl numbers by Müller et al. (1992) using a Ginsburg-Landau equation and by Carrière and Monkewitz (1999) from the calculation of the Green function; the formulae of Müller et al., (1992) involve a small-*Re* expansion whereas those proposed by Carrière and Monkewitz don't. Both critical Rayleigh numbers increase with *Re* for a fixed *Pr* and with *Pr* for a fixed *Re* (Müller et al., 1992; Carrière and Monkewitz, 1999). Concerning the longitudinal rolls, Carrière and Monkewitz (1999) showed that they can only be convectively unstable and that the critical Rayleigh number Ra_c is independent of *Re* and *Pr*: Ra_c is the same as for the

Rayleigh-Bénard problem, namely Ra_c =1707.76, in the case of infinite lateral extension ducts.

The physical model considered here to simulate the PRB flows is shown in Fig. 1. It consists of a horizontal rectangular channel of height H'=1mm, with an aspect ratio L'/H'=10. Initially, the fluid is at a uniform temperature slightly above the critical temperature, $T_i'=(1+\varepsilon)T_c'$ (with $\varepsilon<<1$), and at a mean density equal to the critical density ρ_c', and it flows through the channel according to a Poiseuille profile. Then, the temperature of the bottom wall is gradually increased up to $T_{ch}'=T_i'+\delta T'$ (with $\delta T'$ ranging from about some mK to some hundreds mK) from a distance H' from the channel inlet (Fig. 1).

In a preliminary work (Ameur and Raspo 2013), results were obtained by means of 2D numerical simulations for a supercritical fluid modeled by the Peng-Robinson equation of state at a fixed Reynolds number. They revealed that the thermoconvective patterns observed exhibit characteristics of transversal rolls in spite of the quite large Reynolds number, $Re\approx50$.
In the present paper, 2D numerical simulations based on the computational code presented in Ameur and Raspo (2013) are performed for Reynolds numbers ranging from 12 up to 101 in order to determine the variation of the instability threshold as a function of Re and to characterize more precisely the patterns obtained. The first section is devoted to the mathematical formulation of the problem, the initial and the boundary conditions. Then, the numerical method, based on a Chebyshev collocation approximation, is concisely described. The results are presented in the third section: first we analyze the onset and the evolution of the thermoconvective structures at a fixed distance to the critical point. Then, we investigate the effect of the channel length on these structures and we introduce a stability diagram that summarizes the results obtained. Finally, the influence of the distance to the critical point on the instability threshold is studied. We end up with conclusions based on the results obtained.

2. NUMERICAL MODELS

The supercritical fluid is modeled by the Peng-Robinson equation of state. This equation implicitly accounts for the divergence of the thermal expansion coefficient, β', of the isothermal compressibility, χ', and of the specific heat at constant pressure, C_P', near the liquid-gas critical point. The divergence of the thermal conductivity, λ', is modeled by the formula $\lambda' = \lambda_b'[1+\Lambda(T'/T_c'-1)^{-0.5}]$, where λ_b' is the background term, namely the conductivity in the absence of any critical anomaly (Sengers and Keyes, 1971; Vesovic et al., 1990). The physical parameters of CO_2 were used: T_c'=304.13K, ρ_c'=467.8kg.m^{-3}, Λ=0.75, λ_b'=0.0441265W/m.K.

The evolution of the flow is governed by the time-dependent 2D Navier-Stokes equations coupled with the energy and the Peng-Robinson equations. These equations are solved in the framework of the low Mach number approximation (Paolucci, 1982): the pressure P' is split into a thermodynamic part P_{th}' which is constant in space and appears in the energy equation and in the equation of state, and a dynamic part, P_{dyn}', involved in the momentum equation. However, the basic approximation of Paolucci is modified as proposed by Accary et al. (2005a) to account for the stratification of the fluid near the critical point since Ma^2/Fr (where Ma and Fr are the Mach and Froud numbers, respectively) is not in O(Ma^2). We chose as reference quantities T_c' for temperature, ρ_c' for density, $\rho_c'R'T_c'$ for pressure (with R'=188.92J.kg^{-1}.K^{-1} the perfect gas constant), H' for length, $U_{ref}' = \sqrt{\beta' g' \delta T' H'}$ for velocity (with g' the gravity), H'/U_{ref}' for time and λ_b' for thermal conductivity. The specific heat at constant volume C_V' and the dynamic viscosity μ' were fixed to their background values: C'_{Vb}=632.9J.kg^{-1}.K^{-1} and μ'_b=3.2702×10^{-5}Pa.s. The dimensionless numbers involved are then the Prandtl number, Pr, the Rayleigh number, Ra, the Mach number, Ma and the Froud number, Fr, which are defined by:

$$Pr = \frac{C'_P \mu'_b}{\lambda'_b} \ , Ra = \frac{\beta' g' \rho'^2_c C'_P \delta T' H'^3}{\mu'_b \lambda'_b} \ , Ma = \frac{U'_{ref}}{\sqrt{\gamma_0 R' T'_c}} \ , Fr = \frac{U'^2_{ref}}{g' H'}$$

with γ_0 the specific heat ratio for the perfect gas (γ_0=1.4). In the above formulae, the physical parameters β' and C_P' are calculated from the equation of state for the initial condition (T_i', ρ_i'). The dimensionless governing equations are therefore:

$$\frac{\partial \rho}{\partial t} + \nabla.(\rho \mathbf{V}) = 0 \tag{1}$$

$$\rho \frac{\partial \mathbf{V}}{\partial t} + \rho \mathbf{V}.\nabla \mathbf{V} = -\nabla P_{dyn} + \sqrt{\frac{Pr}{Ra}} \left[\Delta \mathbf{V} + \frac{1}{3} \nabla (\nabla.\mathbf{V}) \right] - \frac{1}{Fr} (\rho - \rho_i) \mathbf{e}_y \tag{2}$$

$$\rho \frac{\partial T}{\partial t} + \rho \mathbf{V}.\nabla T = -(\gamma_0 - 1) T \left(\frac{\partial P}{\partial T} \right)_\rho (\nabla.\mathbf{V}) + \frac{\gamma_0}{Pr_0} \sqrt{\frac{Pr}{Ra}} \nabla.(\lambda \nabla T) \tag{3}$$

$$P_{th} + P_{hyd} = \frac{\rho T}{1 - b\rho} - \frac{a \ \alpha(T) \rho^2}{1 + 2b\rho - b^2 \rho^2} \tag{4}$$

with a and b the dimensionless energy parameter and covolume respectively, and α the Soave function defined by:

$$a = 1.487422 \ , b = 0.253076 \ , \ \alpha(T) = \left[1 + m\left(1 - \sqrt{T}\right) \right]^2$$

where m is computed from the acentric factor ω (ω=0.225 for CO_2) by the following formula:

$$m = 0.37464 + 1.54226\omega - 0.26992\omega^2 .$$

In Eqs. (1)-(4), P_{hyd} is the hydrostatic pressure introduced by the modification of the Low Mach number approximation, $\mathbf{e}_y$ is the unit vector in the *y*-direction and $Pr_0 = \gamma_0 C'_{Vb}\mu'_b/\lambda'_b = 0.6567$.

The initial condition for the dimensionless variables in Ω=[0,*L'/H'*]×[0,1] is:

$$T_i(x,y) = 1+\varepsilon \tag{5}$$

$$u_i(x,y) = 1.5Re\sqrt{\frac{Pr}{Ra}}\left[1-(2y-1)^2\right] \ , \ v_i(x,y) = 0 \tag{6}$$

where *Re* is the Reynolds number defined by $Re = \rho'_c U'_{mean} H'/\mu'_b$, with U'_{mean} the mean velocity at inlet, and *u* and *v* are the velocity components in the *x*- and *y*-directions, respectively. Finally, as it was proposed by Accary et al. (2005a), the stratification of the fluid is taken into account leading to the following initial condition for density and pressure:

$$\rho_i(x,y) = K_2\frac{e^{-K_2 y}}{1-e^{-K_2}} \tag{7}$$

$$P_i(x,y) = P_{thi} + P_{hyd}(y) \tag{8}$$

with

$$K_2 = \gamma_0\frac{Ma^2}{K_1 Fr}, \ K_1 = \frac{1+\varepsilon}{(1-b)^2} - \frac{2a(1+b)\alpha(T_i)}{\left(1+2b-b^2\right)^2}$$

and

$$P_{thi} = \frac{1+\varepsilon}{1-b} - \frac{a\ \alpha(T_i)}{1+2b-b^2} \quad , \quad P_{hyd}(y) = K_1\left[K_2 \frac{e^{-K_2 y}}{1-e^{-K_2}} - 1\right]$$

For velocity components, the no-slip condition and a Poiseuille profile are prescribed on the channel walls and at inlet, respectively:

$$u(x,0,t) = u(x,1,t) = 0 \ , \ v(x,0,t) = v(x,1,t) = 0 \qquad \text{for } 0 \le x \le L'/H' \tag{9}$$

$$u(0,y,t) = 1.5Re\sqrt{\frac{Pr}{Ra}}\left[1-(2y-1)^2\right] \ , \ v(0,y,t) = 0 \qquad \text{for } 0 \le y \le 1 \tag{10}$$

For thermal boundary conditions, the temperature is kept at its initial value, T_i, at inlet and on the top wall (y=1). In order to avoid a discontinuity of the temperature profile on the bottom heated wall (y=0), the following boundary condition is imposed for $0 \le x \le L'/H'$:

$$T(x,0,t) = T_i + \delta T\left[th(2x-2) - th(-2)\right] / \left[th(18) - th(-2)\right] \tag{11}$$

This boundary condition allows a continuous transition between the cold entry zone for $0 \le x \le 1$ and the hot zone corresponding to $1 \le x \le L'/H'$.

In the case of open systems, the choice of good outlet boundary conditions is crucial and it depends on the problem treated. For instance, for the study of instability phenomena, as that considered in this paper, it is necessary to ensure that the perturbation caused by the outlet boundary condition has no effect on the instability onset. Nicolas et al. (1997) compared

several outlet boundary conditions for Poiseuille-Rayleigh-Bénard flows. They showed that Orlanski-type conditions give the best results. Our numerical simulations were therefore performed using these outlet boundary conditions for temperature and velocity components. In terms of dimensionless variables, the boundary condition at $x=L'/H'$ is thus written as:

$$\frac{\partial \phi}{\partial t}\left(L'/H', y, t\right) + Re\sqrt{\frac{Pr}{Ra}}\frac{\partial \phi}{\partial x}\left(L'/H', y, t\right) = 0 \quad \text{for } \phi = T, u, v \quad \text{and } 0 \le y \le 1 \tag{12}$$

3. RESULTS AND DISCUSSIONS

The fluid was set at 1K above its critical temperature. The dimensionless distance to the critical point is thus ε=3.288×10-3 and the Prandtl number is Pr=31.72. Simulations were performed for values of the inlet mean velocity U'_{mean} ranging from 8.83×10^{-4} m/s up to 7.071×10^{-3} m/s, leading to Reynolds numbers varying between 12.6 and 101.1. Temperature increases $\delta T'$ ranging from 1mK up to 100mK were considered so that the resulting Rayleigh number varies between 5.23436×10^{4} and 5.23436×10^{6}.

3.1. Analysis of the thermoconvective structures

In Fig. 2, temperature fields and vertical velocity component contours at different calculation times are presented for Re=12.6 and Ra=6.80466×10^{4}. The contours of v clearly show the perturbation created at the beginning of the heated zone and which grows as it moves downstream. This perturbation finally goes out the computational domain if the simulation is carried out on a sufficiently long time. According to previous theoretical studies on incompressible fluids, this behavior reveals that the flow is convectively unstable. The unstable temperature field exhibits thermal plumes which develop on the hot boundary layer. These structures are similar to those previously obtained for a supercritical fluid in the

Rayleigh-Bénard configuration (Amiroudine et al., 2001; Chiwata and Onuki, 2001; Furukawa and Onuki, 2002; Amiroudine and Zappoli, 2003; Raspo et al., 2004; Accary et al., 2005b; Accary et al., 2005c). However, in a closed cavity, the bottom wall heating induces a piston effect that homogeneously increases the bulk temperature and that gives rise to a second unstable thermal boundary layer on the top cold wall. In the case of the open channel, no piston effect is generated and the heat transfer between the wall and the bulk fluid is only carried out by the thermal plumes. The thermoconvective structures observed are somewhat different for small and large Reynolds numbers. For small values of *Re* (Fig. 2), the temperature fields exhibit a series of identical plumes which are regularly spaced and which occupy the whole height of the channel. The vertical velocity component contours also reveal the presence of regular structures of the same size. On the other hand, for large Reynolds numbers (Fig. 3), only some plumes (mainly three plumes) are observed and the structures are more chaotic: the thermal plumes are tilted in the direction of the forced flow and the contours of *v* are deformed.

The influence of the Reynolds number on the instability onset was studied more precisely for the Rayleigh number $Ra=2.09360\times10^6$ (corresponding to $\delta T'$=40mK) (Fig. 3). In this case, the couple (x'_{ins}, t'_{ins}), where x'_{ins} is the axial position of this first deformation and t'_{ins} the time at which it appears, is ($4H'$, 0.86s) and ($7H'$, 1.14s) for Re=65.7 and Re=101.1, respectively. Figure 3 also shows that the thermoconvective structures are less pronounced when Re is increased: large plumes are observed for Re=65.7 (Fig. 3.a) whereas the perturbation only gives rise to a little deformation of the isotherms for Re=101.1 (Fig. 3.b). These differences of the temperature fields for a same value of the Rayleigh number means that the instability threshold depends on the Reynolds number.

Finally, as we have mentioned at the beginning of this section, all the above results correspond to a convective instability of the flow. However, it must be noted that, for Re=50.6

and a wall heating of $\delta T'$=100mK (corresponding to Ra=5.23436×10^6) the solution obtained in Ameur and Raspo (2013) exhibits the characteristics of an absolute instability: many thermal plumes develop in the whole channel and, as the structures move downstream, new thermal plumes continuously appear near the beginning of the heated zone.

3.2. Stability diagram in (Ra-Re) plane

It is known that, for a fixed value of *Re*, the PRB flow becomes unstable when the Rayleigh number *Ra* exceeds a critical value Ra_c. Linear stability analysis for incompressible flows (Müller et al., 1992, Carrière and Monkewitz, 1999) showed that Ra_c varies with *Re* in the case of transversal rolls whereas it is independent of *Re* in the case of longitudinal rolls. Therefore, the evolution of Ra_c as a function of *Re* gives information about the type of thermoconvective structures obtained. However, the results of these theoretical studies cannot be directly applied to our configuration since they were established with the assumptions of flow incompressibility and constant properties. It is obvious that these assumptions are totally false in the case of supercritical fluids. Nevertheless, for the Rayleigh-Bénard problem (corresponding to the case *Re*=0), Carlès and Ugurtas (1999) showed that the instability criterion established for incompressible flows, namely $Ra>Ra_c$=1707.76, remains valid for supercritical fluids provided that the Rayleigh number *Ra* is replaced by the following modified Rayleigh number:

$$Ra^* = Ra\left(1 - a_g \frac{H'}{\delta T'}\right) \tag{15}$$

where a_g is the adiabatic temperature gradient, $a_g = -\beta' g' T_i'/C_p' = -0.05748\,\mathrm{K/m}$ for $T_i' = T_c' + 1\mathrm{K}$. Thus, we may suppose that, for the PRB problem, instability onset for supercritical fluids is governed by $Ra^*>Ra_c(Re)$ with $Ra_c(Re)$ given by the formulae of Müller

et al. (1992). However, these formulae were established with the assumption of small Reynolds number, which is not the case in the present study.

Consequently, as we couldn't use results of previous theoretical studies, we have investigated numerically the variation of the instability threshold as a function of *Re*. More precisely, for a fixed Reynolds number, successive simulations were performed by increasing gradually the bottom wall heating $\delta T'$ with a maximum increment equal to 2mK until the solution obtained was unstable. Obviously, the Rayleigh number *Ra* for this unstable solution (noted here $\widetilde{Ra}_c$) is not the actual critical Rayleigh number Ra_c but it is slightly larger. The same procedure was applied for several values of the Reynolds number (*Re*=12.6, 50.6, 65.7, 101.1). In Table 1, we report the values of $\widetilde{Ra}_c$ and of its modified version $\widetilde{Ra}_c^*$ (Eq. (15)) which is slightly larger for all the cases.

Results show that the Rayleigh number for the first unstable solution, $\widetilde{Ra}_c$ just as $\widetilde{Ra}_c^*$, increases with *Re*; therefore, the instability threshold depends on the Reynolds number, which confirms that we are still in the range of transversal rolls. We attempted to approximate this threshold by means of a polynomial function of *Re*. Since linear stability analysis showed that the critical Rayleigh number must be an even function of *Re* (Müller et al., 1992), we considered a polynomial of the following form:

$$\widetilde{Ra}_c^*(Re) = a_1 + a_2\, Re^2 + a_3\, Re^4 \qquad (16)$$

The coefficient a_1 is the value of $\widetilde{Ra}_c^*$ for *Re*=0, namely the value for the Rayleigh-Bénard configuration: $\widetilde{Ra}_c^* = Ra_c^* = 1707.76$. The coefficients a_2 and a_3 were fitted on the values of $\widetilde{Ra}_c^*$ for the two highest values of the Reynolds number, *Re*=65.7 and *Re*=101.1, considering that the term in Re^4 is more important as *Re* increases. The resulting values are a_2=112.8425 and a_3=1.9842×10^{-3}. The variation of $\widetilde{Ra}_c^*$ given by Eq. (16) as a function of *Re*, together

with the whole set of couples (*Ra*, *Re*) for which simulations were performed, are shown in Fig. 4. For information purposes, we also drew the critical Rayleigh numbers for the onset of convective instability Ra_{c1} and of absolute instability Ra_{c2} given by the formulae of Müller et al. (1992); we recall that these equations are valid just for $Re<10$ since they were established using a small-*Re* expansion. Figure 4 shows that the Eq. (16) represents quite well the boundary of the convective instability region of the stability diagram in the (*Ra*-*Re*) plane. Therefore, the critical Rayleigh number for the convective instability seems to vary as Re^4 for our configuration. Furthermore, it is clear that the formula of Müller et al. (1992) is not adapted since convectively unstable flows were numerically obtained for much smaller values of *Ra**.

4. CONCLUSION

In this paper, we studied the Poiseuille-Rayleigh-Bénard problem for a supercritical fluid by means of 2D numerical simulations for a wide range of Reynolds numbers from $Re=12$ up to $Re=101$. The thermodynamic state of the fluid is modeled by the Peng-Robinson equation. The temperature fields revealed the existence of thermoconvective instabilities appearing in the form of thermal plumes, similar to those previously observed in the Rayleigh-Bénard configuration. These thermal plumes develop on the hot boundary layer and then move downstream during time. The vertical velocity component contours clearly show the perturbation created at the beginning of the heated zone. When the flow is unstable, this perturbation grows as it moves downstream. In almost all the cases, it finally goes out the computational domain if the simulation is carried out on a sufficiently long time. According to previous theoretical studies on incompressible fluids, this behavior reveals that the flow is convectively unstable.

The influence of the Reynolds number on the convective instability onset and on the development of the structures was studied. The instability threshold was determined from

numerical solutions for several values of *Re* and it was found to vary as a fourth degree polynomial of *Re*.

Acknowledgements.

The authors acknowledge the french 'Agence Nationale de la Recherche' (ANR) for its financial support (White Program ANR-09-BLAN-0105-01). This work was performed using HPC resources from GENCI-IDRIS (grants 2011-20321).

REFERENCES

Accary, G., Raspo, I. Bontoux P., and Zappoli, B., (2005a) An adaptation of the low Mach number approximation for supercritical fluid buoyant flows, *C R Mécanique*, 333, pp. 397-404.

Accary, G., Raspo, I., Bontoux, P. and Zappoli, B., (2005b) Reverse transition to hydrodynamic stability through the Schwarzschild line in a supercritical fluid layer, *Phys. Rev. E*, 72, pp. 035301.

Accary, G., Raspo, I., Bontoux, P. and Zappoli, B., (2005c) Stability of a supercritical fluid diffusing layer with mixed boundary conditions', *Phys. Fluids*, 17, p. 104105.

Ameur, D., Raspo, I., (2013) Numerical simulation of the Poiseuille-Rayleigh-Bénard instability for a supercritical fluid in a mini-channel, *Comput. Thermal Sci*., 5, pp. 107-118.

Amiroudine, S., Bontoux, P., Larroudé, P., Gilly, B. and Zappoli, B., (2001) Direct numerical simulation of instabilities in a two-dimensional near-critical fluid layer heated from below, *J. Fluid Mech.*, 442, pp. 119-140.

Amiroudine, S. and Zappoli, B., (2003) Piston-effect-induced thermal oscillations at the Rayleigh-Bénard threshold in supercritical He, *Phys. Rev. Lett.*, 90, pp. 105301–105303.

Carles, P., Ugurtas, B., (1999) The onset of free convection near the liquid-vapour critical point Part 1: Stationsary initial state, *Physica D*, 126, pp. 69-82.

Carrière, P. and Monkewitz, P. A., (1999) Convective versus absolute instability in mixed Rayleigh-Bénard-Poiseuille convection, *J. Fluid Mech.*, 384, pp. 243-262.

Cansell, F., Aymonier, C., (2009) Design of functional nanostructured materials using supercritical fluids, *J. Super. Fluids*. 47, pp. 508-516.

Chiwata, Y. and Onuki, A., (2001) Thermal plumes and convection in highly compressible fluids, *Phys. Rev. Lett.*, 87, p. 144301.

Cocero, M. J., Martin, A., Mattea, F. and Varona, S., (2009) Encapsulation and co-precipitation processes with supercritical fluids: fundamentals and applications, *J. Supercrit. Fluid*, 47, pp. 546-555.

Furukawa, A. and Onuki, A., (2002) Convective heat transport in compressible fluids, *Phys. Rev. E*, 66, pp. 016302.

Müller, H. W., Lücke, M. and Kamps, M., (1992) Transversal convection patterns in horizontal shear flow, *Phys. Rev. A*, 45, pp. 3714-3726.

Nicolas, X., Traore, P., Mojtabi, A., Caltagirone, J. P., (1997) Augmented Lagragian method and open boundary conditions in 2D simulation of Poiseuille-Bénard channel flow, *Int. J. Numer. Meth. Fluids*, 25, pp. 265-283.

Nicolas, X., (2002) Bibliographical review on the Poiseuille–Rayleigh–Bénard flows: the mixed convection flows in horizontal rectangular ducts heated from below, *Int. J. Therm. Sci.*, 41, pp. 961-1016

Nicolas, X., Zoueidi, N., Xin, S., (2012) Influence of a white noise at channel inlet on the parallel and wavy convective instabilities of Poiseuille-Rayleigh-Bénard flows, *Phys. Fluids*, 24, p. 084101.

Paolucci, S., (1982) On the filtering of sound from the Navier-Stokes equations, *Technical report, Sandia National Laboratories USA, SAND82-8257*.

Raspo, I., Zappoli, B. and Bontoux, P., (2004) Unsteady two-dimensional convection in a bottom heated supercritical fluid, *Comptes Rendus de Mécanique*, vol. 332, pp. 353-360.

Reverchon, E. and De Marco, I., (2006) Supercritical fluid extraction and fractionation of natural matter, *J. Supercrit. Fluid*, 38, pp. 146-166.

Sengers, J.V., Keyes, P.H., (1971) Scaling of the thermal conductivity near the gas-liquid critical point, *Phys. Rev. Lett*., 26, pp. 70-73.

Vesovic, V., Wakeham, W. A., Olchowy, G. A., Sengers, J. V., Watson, J. T. R., Millat, J., (1990) The transport properties of carbon dioxide, *J. Phys. Chem. Ref. Data*, 19, pp. 763-808.

Figure captions

Figure 1: Problem formulation.

Figure 2: Temperature fields and vertical velocity component contours at T'i=T'c+1K (Pr=31.72) for *Re*=12.6 and *Ra*=6.80466×10^4 ($\delta T'$=1.3mK).

Figure 3: Temperature fields and vertical velocity component contours at $T'_i=T'_c$+1K (*Pr*=31.72) for *Ra*=2.09360×10^6 ($\delta T'$=40mK) and two values of *Re*: **(a)** *Re*=65.7, **(b)** *Re*=101.1.

Figure 4: Stability diagram of the PRB flow for a supercritical fluid set at 1K above its critical point. (Δ) Stable flow; (▲) Convective instability; (●) Absolute instability; (——) Polynomial approximation (Eq. (16)) of the threshold; (- - - -) Critical Rayleigh number Ra_{c1} for convective instability for incompressible fluids (Müller et al., 1992); (− − − −) Critical Rayleigh number Ra_{c2} for absolute instability for incompressible fluids (Müller et al., 1992).

Table titles

Table 1: Rayleigh ($\widetilde{Ra}_c$) and modified Rayleigh ($\widetilde{Ra}_c^*$) numbers corresponding to the first unstable solution for supercritical CO_2 set at 1K from the critical point.

Table 1

Re	12.6	50.6	65.7	101.1
$\widetilde{Ra}_c$	2.09374×10^4	4.18749×10^5	5.23436×10^5	1.360933×10^6
$\widetilde{Ra}_c^*$	2.39463×10^4	4.21757×10^5	5.26445×10^5	1.363942×10^6

Figure 1

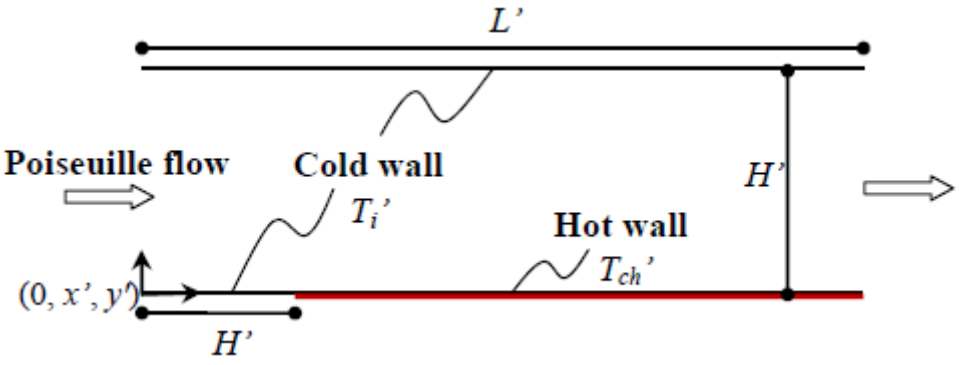

Figure 2

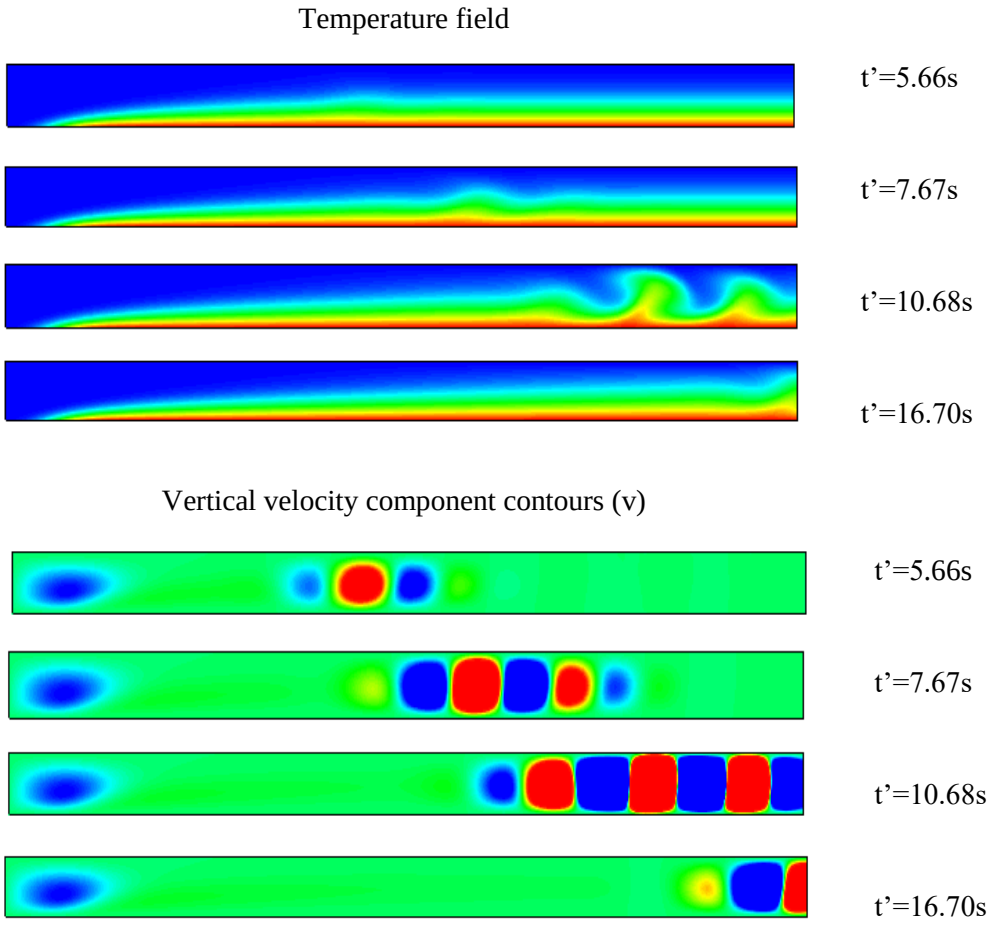
Temperature field
t'=5.66s
t'=7.67s
t'=10.68s
t'=16.70s
Vertical velocity component contours (v)
t'=5.66s
t'=7.67s
t'=10.68s
t'=16.70s

Figure 3

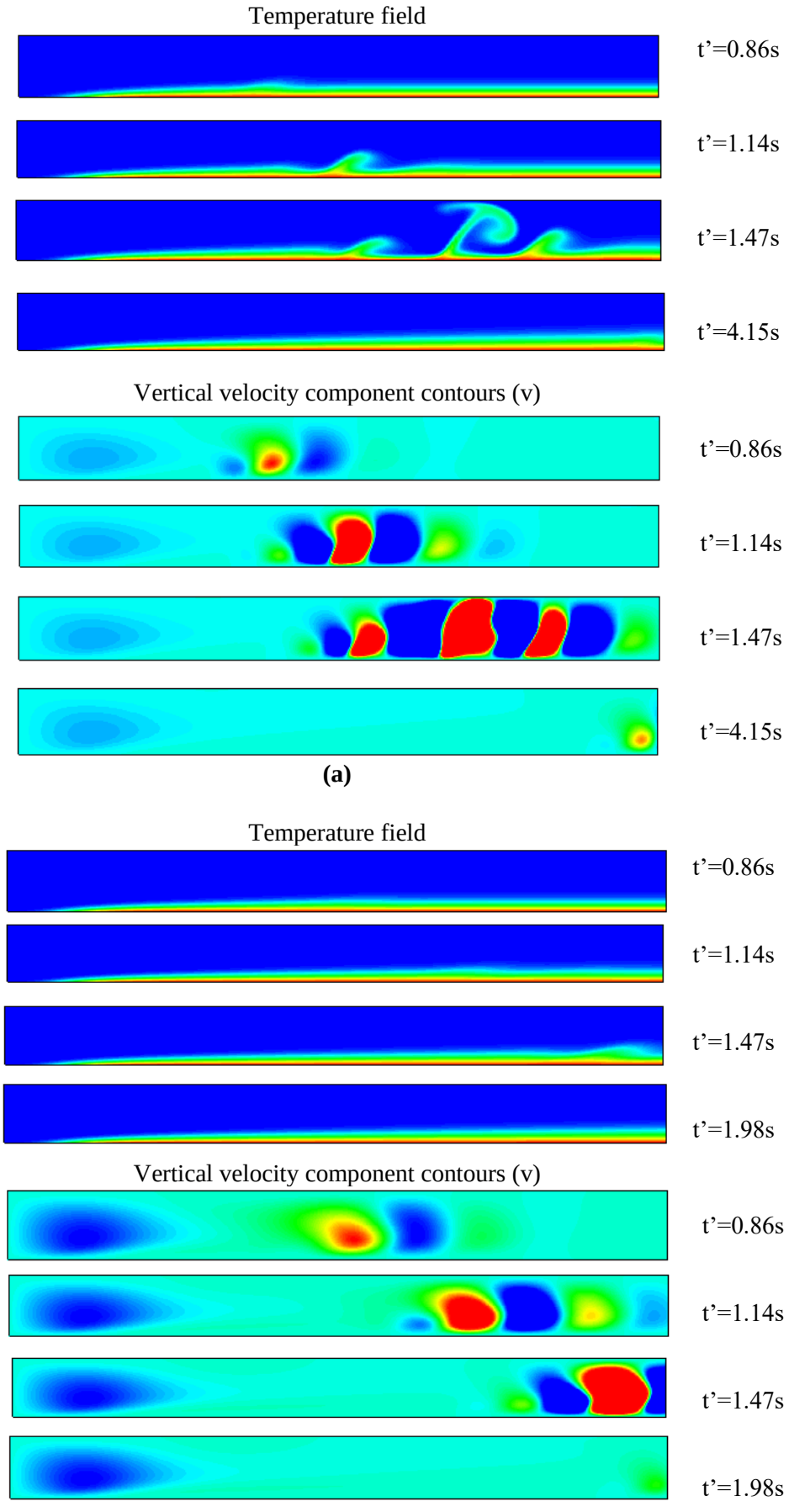
Temperature field
t'=0.86s
t'=1.14s
t'=1.47s
t'=4.15s
Vertical velocity component contours (v)
t'=0.86s
t'=1.14s
t'=1.47s
t'=4.15s
(a)
Temperature field
t'=0.86s
t'=1.14s
t'=1.47s
t'=1.98s
Vertical velocity component contours (v)
t'=0.86s
t'=1.14s
t'=1.47s
t'=1.98s
(b)

Figure 4

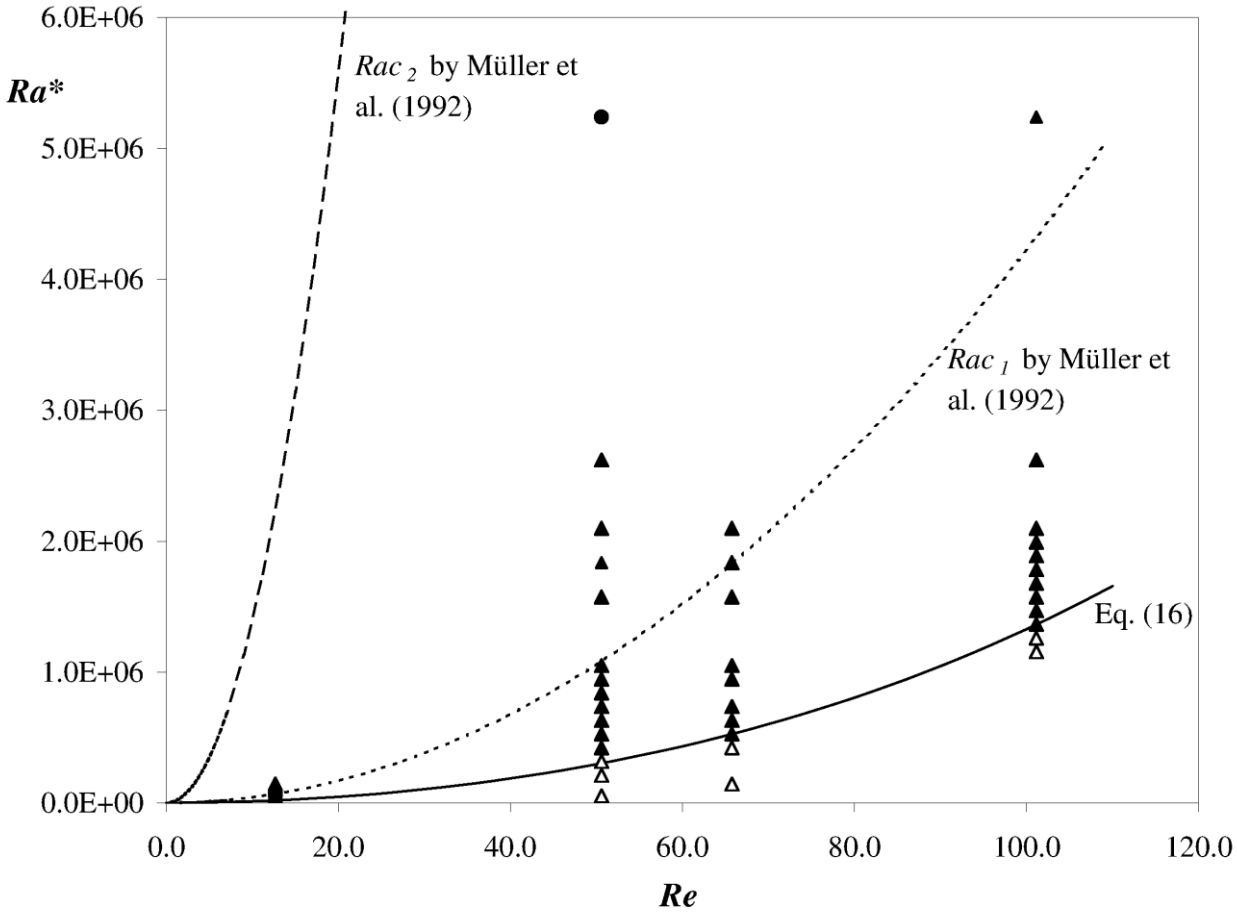
6.0E+06
5.0E+06
4.0E+06
3.0E+06
2.0E+06
1.0E+06
0.0E+00
Ra*
0.0
20.0
40.0
60.0
80.0
100.0
120.0
Re
Rac 2 by Müller et al. (1992)
Rac 1 by Müller et al. (1992)
Eq. (16)